BEST AVAILABLE IMAGES

Defective images within this document are accurate representations of the original documents submitted by the applicant.

Defects in the images may include (but are not limited to):

- BLACK BORDERS
- TEXT CUT OFF AT TOP, BOTTOM OR SIDES
- FADED TEXT
- ILLEGIBLE TEXT
- SKEWED/SLANTED IMAGES
- COLORED PHOTOS
- BLACK OR VERY BLACK AND WHITE DARK PHOTOS
- GRAY SCALE DOCUMENTS

IMAGES ARE BEST AVAILABLE COPY.

As rescanning documents *will not* correct images, please do not report the images to the Image Problem Mailbox.

Society of Petroleum Engineers

SPE 73781

Formation Damage in Iranian Oil Fields

J. Moghadasi, SPE, Petroleum University, University of Surrey, M. Jamialahmadi, SPE, Petroleum University, University of Surrey, H. Müller-Steinhagen, Stuttgart University, A. Sharif, University of Surrey, M.R. Izadpanah, Kerman University

This paper was prepared for presentation at the SPE International Symposium and Exhibition on Formation Damage Control held in Lafayette, Louisiana, 20–21 February 2002.

Abstract

The fine migration and the scale formation into the porous media and the resulting production decline have long been the problem to the petroleum industry. It is also generally accepted that formation due to the particle movement and the scale formation are not thoroughly understood. In contributing to the solution of this problem, an experimentally study of calcium sulphate scale formation and the particle movement in the porous media using of packing bed with 12 different size of the glass and sand bead and the 8 core plug that gathered from the Siri oilfields. The purpose was to study the different physical and mechanical aspects of the processes leading to the formation damage caused by the movement and the entrapment of the suspended particles and the scale formation.

The permeability is the key parameter among several others that control the reservoir performance. The experiments are based on the results of the permeability reduction. The interception of the permeability reduction by the interaction between the operational parameter is very complex. Therefore, several of these factors such as the temperature, the concentration, the fluid dynamic and the type of porous media are considered.

The experimental results are analyzed and a new model which can predicts particle movement and the scaling tendency of the common oilfield water deposits in the water disposal wells, the water flooding systems, and in surface equipment's and the facilities is developed. The developed of the model is based on the experimental data and the empirical correlation, which perfectly mach the Iranian oilfields condition. This model has been applied to the investigate of the potential of the scale precipitation in the Iranian oilfields, either in the onshore or the offshore fields, where the water injection is being performed for the desalting units water disposal purpose or as the method of secondary recovery or the reservoir pressure maintenance.

Introduction

The success of oil recovery is strongly influenced by whether the reservoir permeability can be kept intact or even improved. Permeability changes in petroleum reservoirs have received a great deal of concern by the oil and gas industry. This problem is termed as "formation damage". It can occur during almost any stage of petroleum exploration and production operations. Attempting to understand formation damage is becoming an important task for reservoir engineers, oilfield chemists, and decision-makers in business, because it is first step to be taken to prevent and further alleviate this problem.

Formation Damage Mechanisms-Two phenomena can change the permeability of the rock. One is change of porosity. This phenomenon is due to the swelling of clay minerals or deposition of solids in the pore body. The other is the plugging of pore throats. The narrow passages govern the ease of fluid flow through porous media. If they are blocked, the permeability of the porous rock will be low even though the pore space remains large. Either organic or inorganic matter may cause the plugging of pore throats. The organic induced damage is due to the formation of high viscosity hydrocarbon scale when temperature and pressure conditions in the reservoirs are changed. The inorganic damage involves release and capture of particulate including in situ fines and precipitates from chemical reactions.
The mechanisms that trigger the formation damage can be categorized into three major processes (Leone and Scott, 1987).

Hydrodynamic- A mechanical force mobilizes loosely attached fine particles from the pore surface by exerting a pressure gradient during fluid flow. The movement of clay minerals, quartz, amorphous silica, feldspars, and carbonates may cause mechanical fine migration damage.

Physico-Chemical- This mechanism is induced by the water sensitivity clays. Clays exist in equilibrium with the formation

brine until the ionic composition and concentration of the brine is changed (Crowe, 1986). Double layer forces govern the surface attraction and repulsion between the clay particles and pore wall.

Geochemical- During treatment of reservoirs or waterflooding, the injected fluid may not be compatible with the indigenous pore fluid. This incompatibility results in chemical nonequilibrium in the porous system. The ions contained in the injected fluid may react with the ions in the native fluid to form solid precipitates downstream in the porous system to plug pore throats or to deposit onto pore wall resulting in porosity reduction.

Occurrence of Formation Damage- When fluids are introduced into a porous rock during petroleum exploration and production, its original purpose is to increase the recovery of hydrocarbon. However, due to the incompatibility between injected and indigenous fluids, change of reservoir rock properties can often be expected. The following sections describe the potential causes of formation damage during various oil exploitation activities.

Drilling - During drilling, higher pressure is needed in the wellbore to control the formation being penetrated, the pressure differential will result in invasion of mud solids and mud filtrate into reservoir rock near wellbore. Damage mud solid invasion is strongly influenced by particle size and pore throat size distribution.

Production - The temperature and pressure in the reservoirs are constantly changing during the oil and gas production. Organic scale such as paraffin waxes and asphaltenes may deposit out of the crude oil to plug the formation. Inorganic salts such as calcium carbonate any barium sulfate may also precipitate out of the aqueous phase to block flow paths. The large pressure gradient near the wellbore often is capable of mobilizing fines residing on the surface of pore wall around the producing wells to cause fines migration.

Waterflooding - Compatibility of the injected water with native reservoir fluids is an important factor that influences the success of a waterflooding program. Ions in the source water may react with ions in the reservoir fluids to form insoluble precipitates. Iron corrosion products from injection pipeline and equipment's may generate insoluble compounds, such as iron hydroxide ($Fe(OH)_2$), after mixing with the pore liquid (Krueger, 1986). Pre-filtration of source water is crucial because solids contained in the injected water may induce formation plugging.

Stimulation and EOR - Most stimulation and EOR operations involve chemical treatments. Reactions of different kinds occur when chemicals are introduced into formations. Some of the reactions have adverse effects on formation permeability. During acidizing, acid dissolves iron-containing minerals, such as chlorite, siderite ($FeCO_3$), and hematite (Fe_2O_3). The ferric ions (Fe^{3+}) may precipitate as low soluble ferric hydroxide ($Fe(OH)_3$) upon spending of acid (Crowe, 1985). Acid can also dissolve cementing materials, often carbonates, and liberate sand grains to move within the porous structure and cause permeability reduction (Bryant and Buller, 1988; 1977). Alkaline flooding may be a cost-effective alternative to micellar-polymer flooding to reduce interfacial tension with the natural surfactant formed in situ (Thornton and Lorenz, 1987). Multivalent ions tend to react with alkali to form precipitates. The precipitates include carbonates, hydroxides, and silicates. The common multivalent ions are calcium and magnesium (Krumrine et al., 1985).

In micellar flooding, sulfonate precipitation occurs when the surfactant contacts reservoir fluid that contains inorganic ions. This precipitation may lead to formation plugging (Somasundaran et al., 1984).

A field example is the offshore Siri oil field in Persian Gulf consisted of four platforms A, B, C, and D. It was discovered in 1970 and development drilling began in 1975. Oil production of the field from all the four platforms started in 1978. Total number of the wells drilled was 33 from which 24 were producer, 7 injector and 2 were producer/injector wells. Primary production by natural depletion amounted to 13 MMSTB, which are approximately 2.3% of the total oil in place. Existence of an active aquifer and other appropriate conditions led to the decision of a water injection program. Water injection into the Siri field was stared in 1984 with 9100 bbl/day in order to maintain the pressure and to increase oil recovery. But the injectivity decreased very fast and it reached to 2200 bbl/day in 1990 and consequently the water injection was stopped. The history of water injection in the Siri filed is shown in Figure 1 with a drop in injectivity of approximately 7000 bbl/day over a period of six years. This paper discusses many commonly occurring water quality issues and how they impact injectivity, including damage due to injection of suspended solids, fines migration and formation of insoluble scales and precipitates by an experimental investigation.

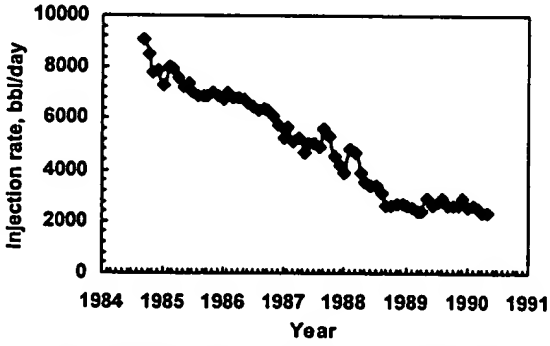

Fig. 1- Water injection history in Iranian Siri oil field

Experimental Apparatus

Experiments were carried out using a test rig, the schematic of which is shown in Figure 2. The prepared suspension flows through a closed looped consisting of a mixing tank, a

reciprocating pump, the test section and the data acquisition system. It consists of the following:

The Tank - It is made of stainless steel. It is heated to approximately 50°C using four band heaters. Each band heater is 40mm wide and has a power rating of 500W @ 240volts.The band heaters are heating against a small cooling coil, which is placed inside the tank, to allow a better control of the liquid temperature in the tank. The cooling coil is made from 20-s.w.g stainless steel tubing, which has an OD of 0.25 inches, and a length of 15 inches. A rotameter is installed to control the cooling water flow rate. The temperature of the liquid inside the tank is determined using a thermocouple which is connected to a controller which in turn will control the band heaters power output. This will hold the temperature at a desired set point. A stirrer is also placed in the tank to agitate the liquid to provide a uniform temperature. The stirrer can rotate between 0-2500 rev./min.

The peristaltic pump - The pump speed ranges from 0.5-55 rpm. so that the liquid flow can be accurately controlled by varying the pump speed which is displayed on a digital screen .The maximum design pressure of the pump is 10 bars which is achieved by utilising a tubing with an internal diameter of 1.6-6.4mm and a wall thickness of 1.6mm.The tubing is made from marprene II, a material which is resistant to water and mineral oil.

Test section - It is a tube made of stainless steel with an internal diameter of 32mm and a wall thickness of 5mm. The total length of the tube is 580mm. Spiral and longitudinal grooves have milled on the outside of the to accommodate heating wire and thermocouples measuring the wall temperature. Bores to insert thermocouples and pressure transducers for measuring the temperature and pressure along the test section. The heating wire is a single core, cold ended heater which is 6m long and 2mm in diameter and is wrapped around the tube at an 8mm pitch. The heating wire is placed inside the 2mm-hemisphere groove and silvers soldered to the tube to keep it in position. The whole heated section is covered in silver solder and lagged so as to reduce heat losses to the surroundings. The heating wire has a hot length of 600cm two cold ends each of 100cm long and two connectors. It has a maximum power output of 2000Watts and a total resistance of 18.06W.The power is controlled to maintain the wall temperature below the maximum operating temperature of around 200°C.Along the tube length there are six pressure transducers and six thermocouples placed at distances .On the same cross section as the third thermocouple from the inlet, there are four thermocouples which are placed inside the longitudinal grooves at an interval of 90° from each other, the averaged value read by them indicate the wall temperature.

Data Acquisition System - It consists of two boards, namely the CIO-DAS08 and the CIO-EXP32 cards which are connected to a desktop computer. The CIO-EXP32 analogue input multiplexer expands the total of analogue input channels of any A/D board by 32 channels. Two banks of 16 analogue inputs, are multiplexed into two of the A/D boards analogue channels. Therefore one bank will be used for inputting thermocouple measurements from the test section, while the other bank will be used for inputting pressure transducer measurements from the test section. The thermocouples and pressure transducers are directly wired into the appropriate banks.

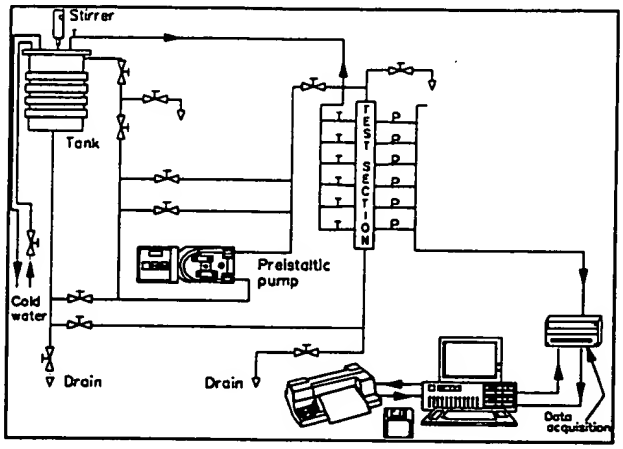

Fig. 2- Schematic diagram of the test rig

Experimental Procedure

All tests were initiated by adjusting the speed of the pump so as to establish a predetermined steady fluid velocity. The power supply was then set to impose a constant rating on the outside of the test section. After rig reached the steady state, the temperature and pressure data were recorded directly into the computer using a Quick Basic program that calculated the permeability. The range of experimental parameters covered in this investigation is summarised in Table 1.

Table1- Range of operating parameters in experiments

Inlet temperature	25-80 °C
Bulk temperature	30-90 °C
Flow rates	1– 200 cm^3/min.
System pressure	1-1000 Kpa
Fluid suspension viscosity	0.790-2 cp.
Specific gravity of Bentonite	2.65 g/cm^3
Specific gravity of Aluminium oxide	3.46 g/cm^3
Suspension concentration of Bentonite	10 – 40 g/l
Suspension concentration of Aluminium oxide	500 – 2000 ppm
Solid particle mixed with packing material	5-10 % wt.
Concentration of $CaSO_4$	0.015 – 0.075 M
Sand and glass bead spherical particle size	250 – 1000 μm

Results and Discussions

Sulphate scaling in Siri fields during water injection-By using of supersaturation index will be shown that in the Siri Field incompatibility problem exist between Persian Gulf,

injection water and Mishrif formation water. Table 2 gives the composition of the Mishrif formation water and Persian Gulf water. The sulphate scaling tendency in the mixed injection. Figure 3 through 7 show the predicted supersaturation of $BaSO_4$, $SrSO_4$ and $CaSO_4$ for Siri– C reservoir. Corresponding to these Figures can be seen that $SrSO_4$ and $CaSO_4$ have tended to formation scale and $BaSO_4$ scale may be formed together. By comparison of Figures 3 with 4 and 5 demonstrates the temperature effect on the sulphate scaling tendencies. An increase in temperature generally, the $CaSO_4$ scaling increases as same as $SrSO_4$ scaling tendencies, thus less gypsum scale and more anhydrate scale will form at higher temperature in this field. The pressure increase universally makes all the sulphate more soluble and therefore less prone to scaling, as indicated from the comparison between Figure 3 and 6 and between Figure 5 and 7. Hence sulphate scale formation may simply result from a pressure drop e.g. as the produced water flow from the reservoir up to the producing wellhead. Figures 8 to 10 show the prediction of sulphate scale formation in Siri Field (Siri –D, Siri-E and Nosrat) in various temperature and pressure. Summary of prediction of scale formation in Siri Filed at reservoir conditions and various temperature and pressure conditions are presented in Table 3.

Table 2- Water analysis of Persian Gulf water and Mishrif formation water in Siri Field

Ions (mg/l)	Siri- C	Siri- D	Siri- E	Nosrat	Sea Water
Cl^-	73942	70740	83324	86900	23000
SO_4^{-2}	635	310	142	340	3350
HCO_3^-	579	528	397	244	166
Mg^{+2}	759	766	552	2010	2996
Ca^{+2}	3032	4525	8917	7920	267
Na^+	42215	35391	42800	43700	11750
K^+	1986	-	88	-	-
Ba^{+2}	-	-	-	18	0.09
Fe^{+2}	17	5.6	246	-	0.42
Sr^{+2}	547	760	-	610	3.4
Li^+	-	-	-	-	-
TDS	131472	129225	137370	141000	40270
PH	6.82	5.86	6.25	5.6	7.7
CO_2	-	100	-	-	-
H_2S	-	14	-	-	-

Table 3 – Summary of prediction of scale formation in Siri Field (Siri- C, Siri- D, Siri- E and Nosrat)

Reservoir	T, °C	P, psi	Type of scale
Siri- C	100	270	$SrSO_4$, Anhydrate (Reservoir condition)
	70	270	$SrSO_4$
	50	270	$SrSO_4$, Anhydrate
	100	135	$SrSO_4$
	50	135	$SrSO_4$
Siri- D	103	270	$SrSO_4$, Anhydrate (Reservoir condition)
	50	60	$SrSO_4$, Anhydrate
Siri- E	100	270	Gypsum,Anhydrate(Reservoir condition)
	50	135	Gypsum, Anhydrate
Nosrat	100	270	$BaSO_4$, $SrSO_4$, Anhydrate
	50	135	$BaSO_4$, $SrSO_4$

Scale formation in sand pack porous medium- Figure 11 shows that until 1.3 pore volume injected the permeability ratio approximately constant and then very rapidly decrease. It shows that the calcium sulfate crystallization occurred in the inlet section of porous media and caused that restricted for flowing of fluid. Therefore permeability ratio reduction is very fast. Figure 12 shows that when concentration of calcium sulfate increase to 0.075 M, after 0.3 pore volume injected the reduction of permeability ratio become very fast and then it reaches to 0.01. Figure 13 shows when concentration of calcium sulfate kept constant to .075 and injection flow rate is increased to 25 cm^3/min, trend of permeability ratio reduction is slower than before case that flow rate was 10 cm^3/min. This shows that by increases of flow rate, the value of supersaturetion increased, consequently the rate of precipitation, crystal growth and plugging is rapidly raised and a sharply decrease in permeability ratio.

Scale formation in glass bead porous medium- For preventing of any chemical or mechanical interaction that may be occurred between sand and injected solution, glass bead media is chosen as porous media. In following experimental results, which are done in various temperature, concentration and flow rates.

Effect of temperature- The role of temperature on the solubility and crystal growth of calcium sulphate is very important. These series of experiment are done at three different temperatures and the flow rate are kept constant in 25 cm^3/min. Figure 14 shows that the effect of temperature on permeability reduction. As temperature raises, the rate of nucleation and crystal growth and plugging are increased. Consequently in higher temperature, the rate of permeability ratio reduction becomes faster.

Effect of concentration- To investigate the effect of calcium sulphate concentration on the permeability reduction, three tests were considered, in which the rate of injection solution and temperature was remained constant but the concentration solution was 0.015 M, 0.025 M and 0.075 M. Figure 15 shows the effect of concentration on permeability ratio reduction. A concentration is increased the supersaturation of solution raises and the rate of nucleation and crystal growth raised. Therefore by increasing of concentration, the rate of reaction, nucleation, crystal growth and plugging are increased.

Particle movement in glass bead porous medium- The experiment runs performed were aimed to determine the effect of different parameters on the permeability reduction due to particle movement in the porous media. These parameters are concentration of solid suspension particles, flow rate and solid particle, which initially presented in the porous medium. Effect

Effect of injection flow rate- To investigate the effect of injection flow rate on pressure drop and permeability reduction a set of tests were performed, in which the concentration of solids in the injected water was kept at a

constant value of 30g/l while the injection rate was varied in each test. Figure 16 shows that the rates of permeability reduction increase sharply as the flow rate increases. The reason for this behavior may be do to the fact that the rate of plugging increase as the flow rate increase.

Effect of solid particle concentration- To study the effect of the concentration of solid particles in the injection water on the permeability reduction, a number of tests were carried out. In these experiments, the rate of injection fluid was kept constant and the concentration of the solid particles in the injecting fluid was varied. These tests were carried out at constant injection rate of 50 cm^3/min and three different solids concentrations of 20 g/l, 30 g/l and 40 g/l. Variation of permeability ratio as a function of pore volume injected is shown in Figure 17. By increasing the concentration of solid particles in injecting fluid, sedimentation and plugging occurs more rapidly and consequently, the permeability reduction decreases more rapidly.

Effect of solid particles initially present in porous medium- Before starting the water injection, some particles is present in the porous medium. When the water is injected into the porous medium and the water velocity reaches the mobilization velocity, these particles move and cause some plugging, therefore, reducing the permeability of the porous medium. To investigate the effect and the role of this phenomenon on permeability reduction, the following experiments are performed. In the first run, the glass bead medium was filled with 4.5% wt. alumina particles of 7 μm particle size. Pure water was then injected into the glass bead medium. As the water flows in the medium, the alumina particles move ahead and cause throat plugging. Consequently, as it is shown in Figure 18, the pressure gradient across the glass bead medium increases. It can be seen that the pressure increases initially very smoothly and then starts to increase more rapidly. As the pressure reaches a certain value, the pressure of the system starts to fluctuate. This fluctuation in pressure may indicate the breaking of the plugs of the throats. Figure 19 shows the behavior of the system permeability as the water is injected. As before, a slow permeability decrease in the glass bed is observed, and then this decrease in permeability proceeds faster, and after about 140 minutes fluctuation in permeability is recognized. This fluctuation is due to the breaking of the bridges in the throats of the porous medium.

Mathematical model to describe particle movement and deposition in porous media- The phenomenon of solid particles invasion and capture in a porous medium is a subject that is encountered in reservoir engineering applications. A mathematical model is obviously necessary to theoretically explain the underlying phenomena. An attempt to describe the phenomenon of formation damage caused by solid particles invasion and capture in a porous medium and the subsequent permeability alteration is one of the reasons to develop a new mathematical model in this study. The mathematical expressions derived in this study are obtained by conceptually representing an actual porous medium using a porous model based on the following fundamental and general assumptions:

1. Solid particles are uniformly suspended in an incompressible fluid.
2. The porous medium is homogeneous and isotropic.
3. The porous medium contains a large number of pore bodies, which are interconnected by pore throats whose sizes are log-normally distributed.
4. The interaction forces between the glass bead and the suspended solids are not accounted.
5. The fluid containing solid particles is injected into a porous medium at a constant flow rate.

Consider an element of the porous medium of length Δx and cross-sectional area A with effective initial porosity,ϕ_i, (Figure 22).

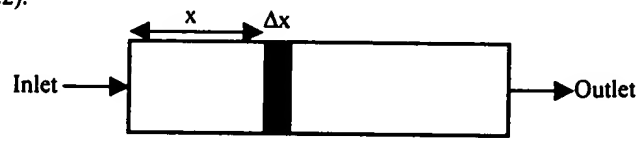

Fig. 22- Schematic diagram of linear model

The particle material balance on the stream of fluid flowing through the elemental porous medium can be represented by the following expressions:

$$-\frac{\partial}{\partial x}\left(QC_s - D_s A\phi\frac{\partial}{\partial x}C_s\right)\Delta x = A\Delta x\phi\frac{\partial}{\partial t}C_s \qquad (1)$$

Based on the operating conditions observed in the experiments, the pore space of the porous medium is occupied by saturating fluid. Initially, the concentration of solid particles is set to zero, therefore:

$$C_s(x,0) = 0 \qquad (2)$$

$$C_s(0,t) = C_{si} \qquad (3)$$

$$C_s(\infty,t) = 0 \qquad (4)$$

The solution of the equation (1) using the above initial and boundary conditions yields:

$$C_s(x,t) = \frac{1}{2}C_{si}\left\{\operatorname{erfc}\left(\frac{x\phi - ut}{\sqrt{4D_s t}}\right) + \exp\left(\frac{ux}{D_s}\right)\operatorname{erfc}\left(\frac{x\phi + ut}{\sqrt{4D_s t}}\right)\right\} \qquad (5)$$

Using similar methods as for solving equation (1), in a radial system can be written as:

$$C_s(r,t) = C_{si}\exp\left[\alpha(r - r_0) + \sqrt{\frac{\beta}{D_s}}(r - r_0) + 2\beta t\right] \qquad (6)$$

Where:

$$\alpha = \frac{1}{2D_s}\left(\frac{D_s}{r} - \frac{Q}{\gamma}\right), \beta = \frac{1}{4D_s}\left(\frac{D_s}{r} - \frac{Q}{\gamma}\right)^2 \text{ and } \gamma = 2\pi hr\phi \qquad (7)$$

Due to solid particle invasion into a porous medium, the porosity of the porous medium will change. The instantaneous porosity is calculated with the following equation

$$\phi = \phi_i - \phi_s \qquad (8)$$

Kumar and Todd (1988) developed a relationship between solid particles, C_s and instantaneous porosity. This relationship is used in this model.

$$\phi = \phi_i - \phi_s = \left(\frac{C_{si} - C_s}{\rho_s - C_s}\right).\phi_i \qquad (9)$$

The following power law relationship using initial and instantaneous porosity has been suggested by Civan et al. (1988). This model is used to predict the instantaneous value of porosity in the developed model.

$$\frac{k}{k_i} = \left(\frac{\phi}{\phi_i}\right)^3 \qquad (10)$$

Validation of the phenomenological model-The phenomenological model developed in this study is intended to predict the behavior of solid particles contained in water during injection into a porous medium. The model is validated using parameters, which are employed in the experiments, and the results are compared with experimental data. The results exhibit a clear trend of permeability decline. This trend increases as the flow rate increases. When the concentration of solid particles increases, the level of permeability damage is also increased and a large difference exists at low concentration. These effects are clearly shown in Figures 21-22.

Conclusions

The current research has been successful in achieving several important goals:

1. Permeability decline is affected by the following parameters: solid particle concentration, flow rate, and the initial permeability of the porous medium. The high rates of permeability damage occurred under conditions of high concentration of solid particles, small ratio of solid particle size to the mean diameter as well as low flow rates in low permeability porous media.
2. Low permeability porous media are more sensitive to permeability damage caused by solid particles invading pore spaces than high permeability porous media.
3. Solid particles initially present in the porous medium perform an important role when the water is injected into porous media
4. The phenomena of the invasion of solid particles into a porous medium were simulated by the use of a phenomenological mathematical model. The modeling results provided same information for understanding the mechanisms of permeability alteration resulting from solid particle invasion into a porous medium.
5. The presented model is capable of simulating invasion of solid particles through the porous medium. The modeling results obtained from running the phenomenological model demonstrated that this model could predict the trend of permeability damage due to the invasion of solid particles.
6. The modeling results demonstrate a close agreement with experimental data.
7. The radial model predicts permeability reduction in radial porous media.
8. The injection rate has a significant effect on the permeability reduction. The effect is different from what is reported for pipelines. In the porous medium, as the injection rate is increased, the rate of pressure drops increase too. This shows that the increase of injection rate in porous media leads to faster and more severe permeability reduction during water injection.
9. The amount of solid particles that are carried by the injection water into the porous medium is another important factor. Unfortunately, we could not do any tests with specified particle sizes. However, some tests were carried out with different solid particle concentrations in the injecting water. The results show that as the concentration of solid particles is reduced, the permeability reduction takes a longer time. Based on these results the importance of filtration of the injecting water is confirmed.
10. Injection zone: from the results of the tests and upon comparison of permeability reduction curves of the overall system and the of middle part, it is concluded that permeability reduction takes place mostly in the inlet zone of the injected medium. By this we mean that permeability reduction is more severe near the injection point. The formation damage due to permeability impairment takes place in the first few centimeters of the system and deeper parts of the system are less important for the overall permeability reduction of the whole system.

Based on experiments it is concluded that solid particles that are initially present in the porous medium can cause permeability reduction in the porous medium during water injection. The injection water can mobilize these particles and these mobilized particles can subsequently cause permeability reduction. One of the important factors in permeability reduction due to the movement of internal solid particles is the sticking factor. If the solid particles are more strongly attached to the pore wall surface, then the required injection velocity for mobilizing the particles is higher.

Nomenclature

A	cross-sectional area, m^2
C_s	mass solid concentration, kg/m^3
dp/dx	pressure gradient in x direction, N/m^3
D_s	Diffusion coefficient, m^2/s
h	depth, m
K	permeability, m^2
L	average length of flow path, m
p	pressure, N/m^2
Q	volumetric flow rate, m^3/s

r	radial distance, m
r_o	radius, m
r_w	well bore radius, m
T	temperature
TSS	total suspended solids
t	time, s
u	velocity flowing phase through porous media, m/s
V	volume, m^3
x	distance from inlet face of core

Greek Symbols

ϕ	porosity
μ_l	viscosity of the carrier liquid, kg/m.s
ρ	fluid mass density, kg/m^3
ρ_s	particle grain density, kg/m^3

Subscripts

°	core inlet, stagnant or initial
bbl	barrel
i	initial or inlet
in	inlet
l	liquid
L	length
out	out let side
Pa	Pascal (N/m2)

References

1. Bryont, S.L. and Buller, D.C.: "Formation Damage from Acid Treatments," Paper SPE 17597 Presented at the SPE International Meeting on Petroleum Engineering, Tianjin, China, Nov. 1-4, 1988.
2. Crow, C.W.: "Evaluation of Agents for Preventing Precipitation of Ferric Hydroxide From Spent Treating Acid," JPT (Apr. 1985) 691-695.
3. Crow, C.W.: "Precipitation of Hydrate Silica From Spent Hydrofluoric Acid," JPT (Nov. 1986) 1234-1240.
4. Krueger, R.F.: "An Overview of formation Damage and Well Productivity in Oil Field Operation," JPT (Feb. 1986) 131-152.
5. Krumine, P.H., Mayer, E.H. and Brock, G.E.: "Scale Formation During Alkaline Flooding," JPT (Aug. 1985) 1466-1474.
6. Kumar, T. and Todd, A.C.: "A New Approach for Mathematical Modeling of Formation Damage Due to Invasion of Solid Suspensions," paper SPE 18203 Presented at the 63rd Annual Technical Conference and Exhibition of the Society of Petroleum Engineers, Houston, TX, October 2-5, 1988.
7. Leon, J.A. and Scott, E.M.: "Characterization and Control of Formation Damage During Water Flooding at High Clay content Reservoir," Paper SPE 16234 Presented at the SPE Production Operation Symposium, Oklahoma City, OK, Mar. 8-10, (1987).
8. Somasundaran, P., Celik, M., Goyal, A. and Manev, E.: "The Role of Surfactant Precipitation and Redissolution in the Adsorption of Sulfonate on Minerals," SPEJ, (Apr. 1984), 233-239.
9. Thronton, S.D. and Lorenz, P.B.: "Role of Silicate and Aluminate Ions in the Reaction of Sodium Hydroxide with Reservoir Minerals," Paper SPE 16277 Presented at the SPE International Symposium on Oilfield Chemistry, San Antoni, TX, Feb. 4-6, 1987.

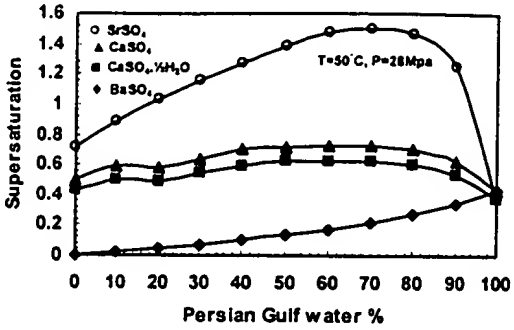

Fig. 3- Prediction of Sulphate scale formation from mixing of Siri-C formation water and Persian Gulf

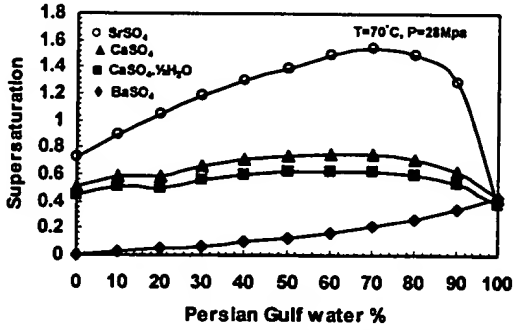

Fig. 4- Prediction of Sulphate scale formation from mixing of Siri-C formation water and Persian Gulf

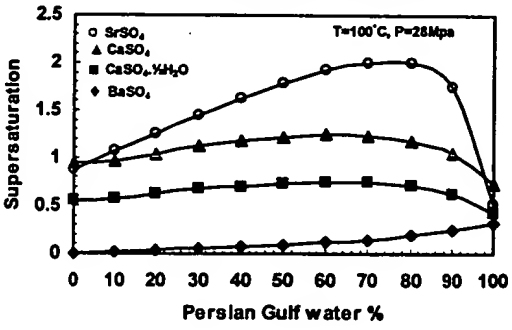

Fig. 5- Prediction of Sulphate scale formation from mixing of Siri-C formation water and Persian Gulf

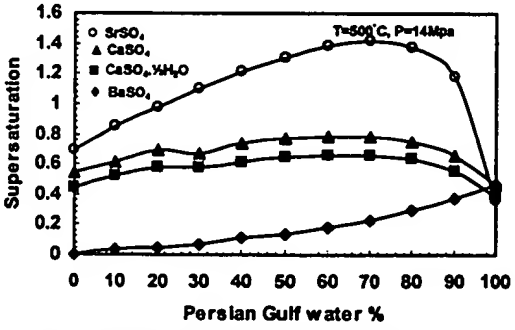

Fig. 6- Prediction of Sulphate scale formation from mixing of Siri-C formation water and Persian Gulf

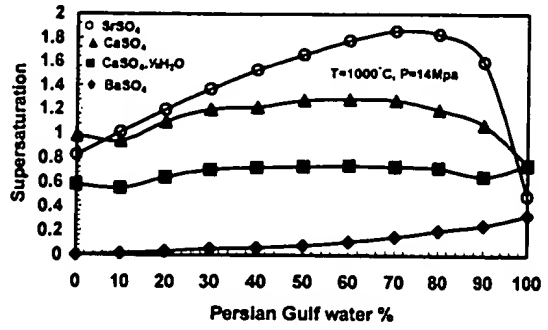

Fig. 7- Prediction of Sulphate scale formation from mixing of Siri-C formation water and Persian Gulf

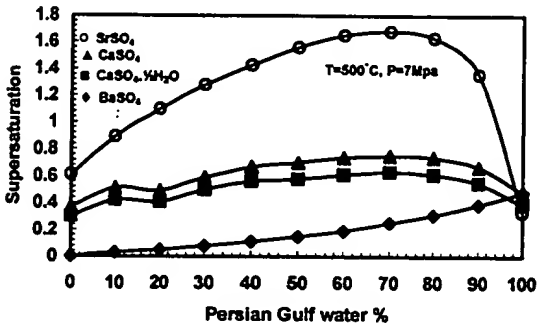

Fig. 8- Prediction of Sulphate scale formation from mixing of Siri-D formation water and Persian Gulf

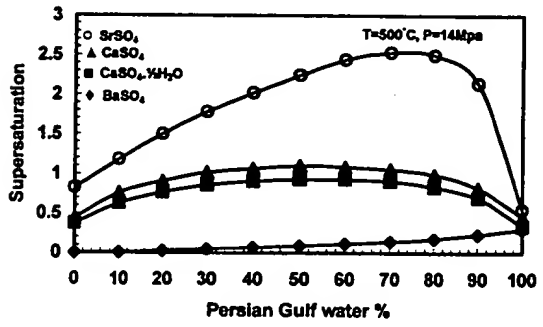

Fig. 9- Prediction of Sulphate scale formation from mixing of Siri-E formation water and Persian Gulf

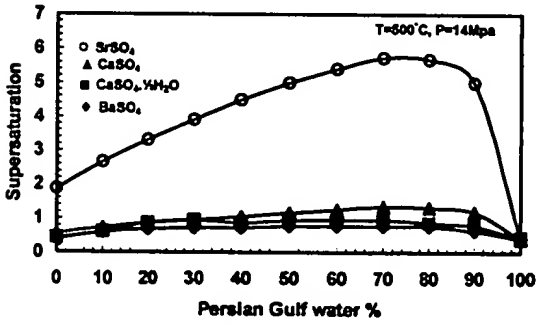

Fig. 10- Prediction of Sulphate scale formation from mixing of Siri-Nosrat formation water and Persian Gulf

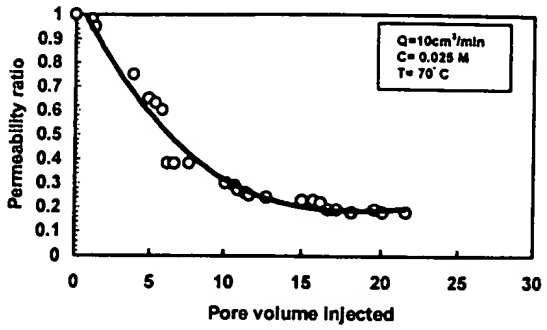

Fig. 11- Variation of permeability ratio as a function of pore volume during calcium sulphate solution injecetd

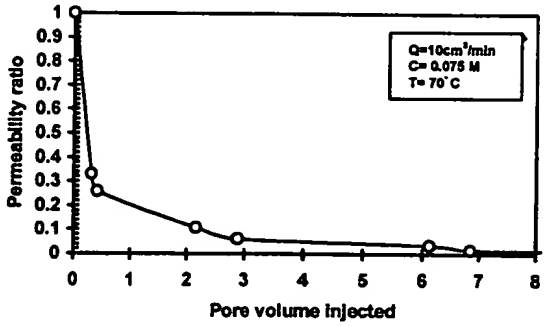

Fig. 12- Variation of permeability ratio as a function of pore volume during calcium sulphate solution injecetd

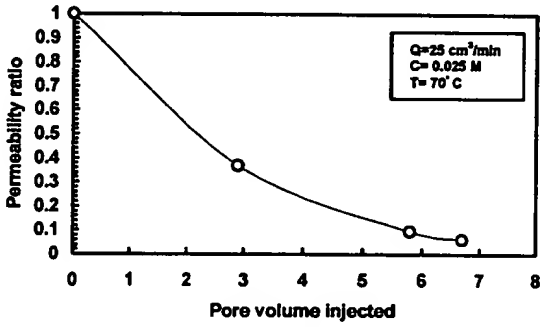

Fig. 13- Variation of permeability ratio as a function of pore volume during calcium sulphate solution injecetd

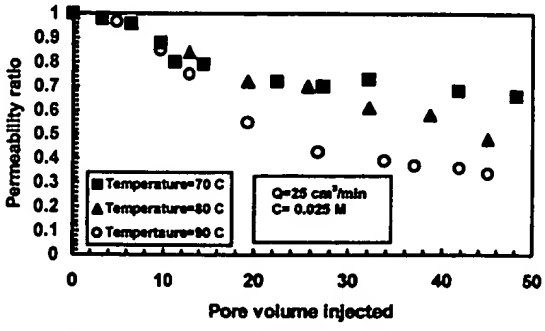

Fig. 14- Variation of permeability ratio as a function of pore volume during calcium sulphate solution injecetd

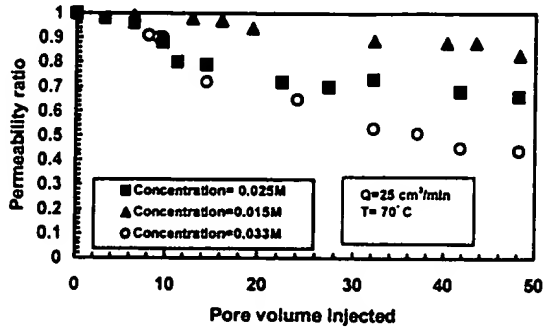

Fig. 15- Variation of permeability ratio as a function of pore volume during calcium sulphate solution injecetd

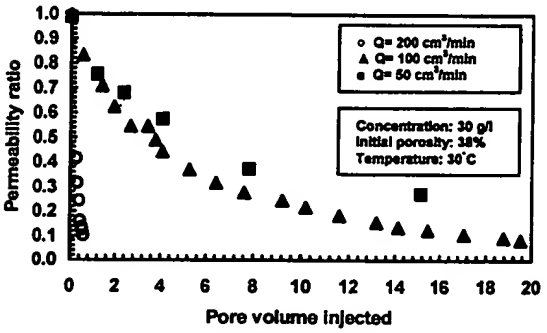

Fig. 16- Variation of permeability ratio as a function of pore volume

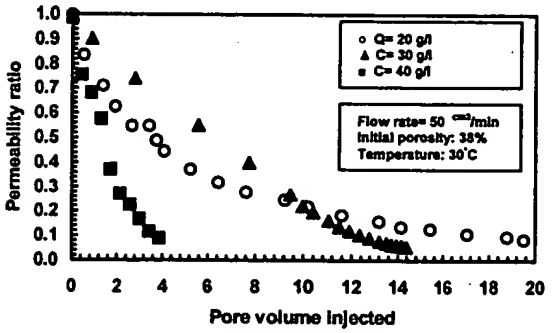

Fig. 17- Variation of permeability ratio as a function of pore volume

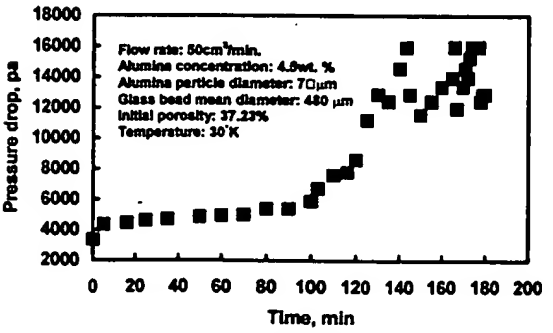

Fig. 18- Variation of permeability ratio as a function of time

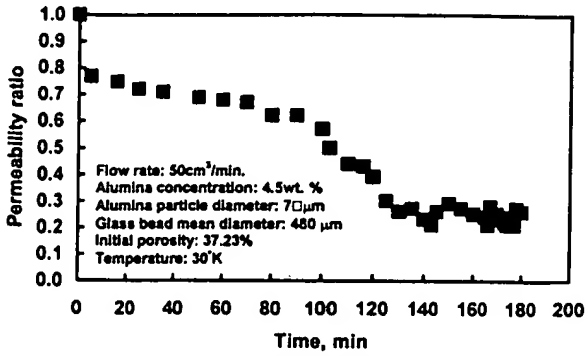

Fig. 19- Variation of permeability ratio as a function of pore volume

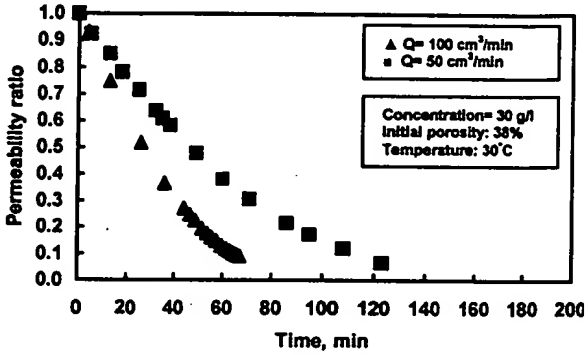

Fig. 20- Variation of permeability ratio as a function of pore volume

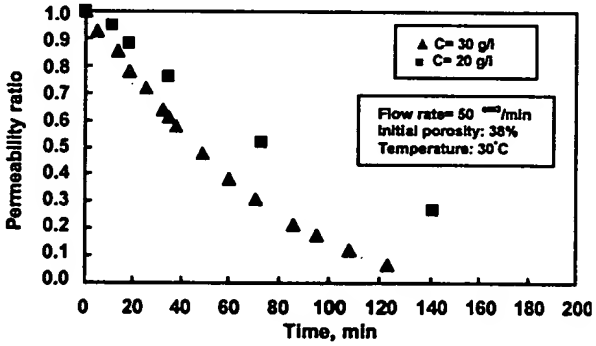

Fig. 21- Variation of permeability ratio as a function of pore volume